

See discussions, stats, and author profiles for this publication at: <https://www.researchgate.net/publication/274699422>

# Unraveling the Effect of PbI<sub>2</sub> Concentration on Charge Recombination Kinetics in Perovskite Solar Cells

ARTICLE · MARCH 2015

DOI: 10.1021/ph500255t

---

CITATION

1

READS

312

## 4 AUTHORS, INCLUDING:



Ahmed M. El-Zohry

Uppsala University

21 PUBLICATIONS 102 CITATIONS

SEE PROFILE



Anders Hagfeldt

École Polytechnique Fédérale de Lausanne

391 PUBLICATIONS 31,907 CITATIONS

SEE PROFILE



Gerrit Boschloo

Uppsala University

197 PUBLICATIONS 14,077 CITATIONS

SEE PROFILE

# Unraveling the Effect of $\text{PbI}_2$ Concentration on Charge Recombination Kinetics in Perovskite Solar Cells

Dongqin Bi,<sup>†</sup> Ahmed M. El-Zohry,<sup>†</sup> Anders Hagfeldt,<sup>†,‡</sup> and Gerrit Boschloo\*,<sup>†</sup>

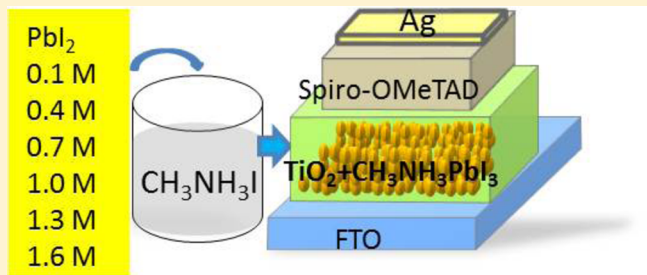
<sup>†</sup>Department of Chemistry-Ångström Laboratory, Uppsala University, Box 532, SE 751 20 Uppsala, Sweden

<sup>‡</sup>School of Chemical Engineering, Sungkyunkwan University, Suwon 440-746, Korea

## Supporting Information

**ABSTRACT:**  $\text{CH}_3\text{NH}_3\text{PbI}_3$  perovskite solar cells have rapidly risen to the forefront of emerging photovoltaic technologies. A solution-based, two-step method was reported to enhance the reproducibility of these solar cells. In this method, first a coating of  $\text{PbI}_2$  is applied by spin-coating onto a  $\text{TiO}_2$ -coated substrate, followed by a dip in a methylammonium iodide solution, leading to conversion to  $\text{CH}_3\text{NH}_3\text{PbI}_3$ . The concentration of  $\text{PbI}_2$  in the spin-coating solution is a very important factor that affects the infiltration of the perovskite and the amount deposited. The best solar cell performance of 13.9% was obtained by devices prepared using 1.0 M of  $\text{PbI}_2$  in dimethylformamide. These devices also had the longest electron lifetime and shortest carrier transport time, yielding lowest recombination losses. Rapid quenching of the perovskite emission is found in device-like structures, suggesting reasonably good efficient carrier extraction at the  $\text{TiO}_2$  interface and quantitative extraction at the spiro-OMeTAD interface.

**KEYWORDS:**  $\text{CH}_3\text{NH}_3\text{PbI}_3$ , recombination, emission lifetime, hybrid photovoltaics



Evolving from dye-sensitized solar cells (DSSCs),<sup>1</sup> organo-metal halide perovskites solar cells promise to deliver one of the lowest cost technologies that is capable of converting sun light to electricity at the highest efficiencies.<sup>2</sup> The most efficient perovskites used in solar cells to date are  $\text{CH}_3\text{NH}_3\text{PbX}_3$  ( $X = \text{I}^-$ ,  $\text{Br}^-$ ,  $\text{Cl}^-$ ). In this compound, each  $[\text{PbX}_6]^{4-}$  octahedron is connected with six neighbors at the iodide to form a multiple quantum well structure, with  $[\text{PbX}_6]^{4-}$  functioning as the quantum well and the  $\text{CH}_3\text{NH}_3^+$  layer as the barrier.<sup>3,4</sup> Substitution of the organic cations, that is,  $(\text{HC}(\text{NH}_2)_2)^{2+}$ ,<sup>5–7</sup>  $\text{CH}_3\text{CH}_2\text{NH}_3^+$ ,<sup>8</sup> and a mixture of  $\text{CH}_3\text{NH}_3^+$  and  $(\text{HC}-(\text{NH}_2)^{2+})$ ,<sup>9</sup> metal cations, that is,  $\text{Sn}^{2+}$ ,<sup>10</sup> and halide anions, that is,  $\text{Br}^-$ ,<sup>11,12</sup> and a mixture of  $\text{Cl}^-$ ,  $\text{Br}^-$ , and  $\text{I}^-$ ,<sup>13–15</sup> have been applied in perovskite solar cells. Although a higher open-circuit voltage ( $V_{oc}$ ) or short-circuit current ( $J_{sc}$ ) has been achieved from such trials, the overall solar cell device performances still lag behind the ones made from  $\text{CH}_3\text{NH}_3\text{PbI}_3$  or  $\text{CH}_3\text{NH}_3\text{PbI}_{3-x}\text{Cl}_x$ . The highest power conversion efficiency (PCE) of perovskite solar cell has been approached to 17.9% within two years.<sup>16</sup> The fast pace is mainly due to improvements of the deposition method for perovskites.

Much of the initial work on  $\text{CH}_3\text{NH}_3\text{PbI}_3$  and  $\text{CH}_3\text{NH}_3\text{PbI}_{3-x}\text{Cl}_x$  solar cells utilized spin-coating to deposit perovskites from a single solution onto a mesoporous metal oxide substrate.<sup>17–20</sup> When spin-coating, the excess solution on top of the film can act as a reservoir. The infiltration of the perovskite depends critically on film thickness, solvent, solution concentration, and spin-coating speed.<sup>21</sup> The crystallization tendency of the perovskite films could lead to rough surface

morphologies which could introduce shunts into the solar cells.<sup>22</sup> The perovskite was found to work very well not only on mesoporous semiconductors, such as  $\text{TiO}_2$ ,<sup>17</sup> and  $\text{ZnO}$ ,<sup>20</sup> but also on insulator scaffolds such as  $\text{Al}_2\text{O}_3$ ,<sup>18</sup> and  $\text{ZrO}_2$ .<sup>28</sup> Aiming to improve the film morphology and the infiltration of perovskite, various other methods have been applied. Efficient planar perovskite solar cells (15.4%) formed by dual source evaporation of  $\text{PbCl}_2$  and  $\text{CH}_3\text{NH}_3\text{I}$  were first demonstrated by Snaith and co-workers.<sup>23</sup> Bolink and co-workers obtained efficiencies of 12.0% using dual source evaporation of  $\text{PbI}_2$  and  $\text{CH}_3\text{NH}_3\text{I}$ .<sup>24</sup> A vapor-assisted solution process (VASP) reported by Yang et al. was used to obtain planar solar cells with an efficiency of 12.1%.<sup>25</sup>

A significant development in solution based deposition is the two-step method originally developed by Mitzi and co-workers<sup>26</sup> to make perovskite solar cells.<sup>27,28</sup> Up to now, a two-step method has been reported to be an effective way to make highly reproducible and efficient Au/spiro-OMeTAD/ $\text{CH}_3\text{NH}_3\text{PbI}_3/\text{m-TiO}_2$ (mesoporous)/d- $\text{TiO}_2$ (dense)/FTO solar cells.<sup>27</sup> It is likely that the  $\text{PbI}_2$  layer deposited on top of mesoporous substrates has increased roughness that allows the conversion reaction to proceed faster. Considering the volume expansion (~75%)<sup>25</sup> occurring due to the conversion of  $\text{PbI}_2$  into  $\text{CH}_3\text{NH}_3\text{PbI}_3$ , it can be expected that the mesoporous scaffold layer would be better filled using the two-step method. Recently, it has been reported that the presence of  $\text{PbI}_2$  can

Received: July 15, 2014



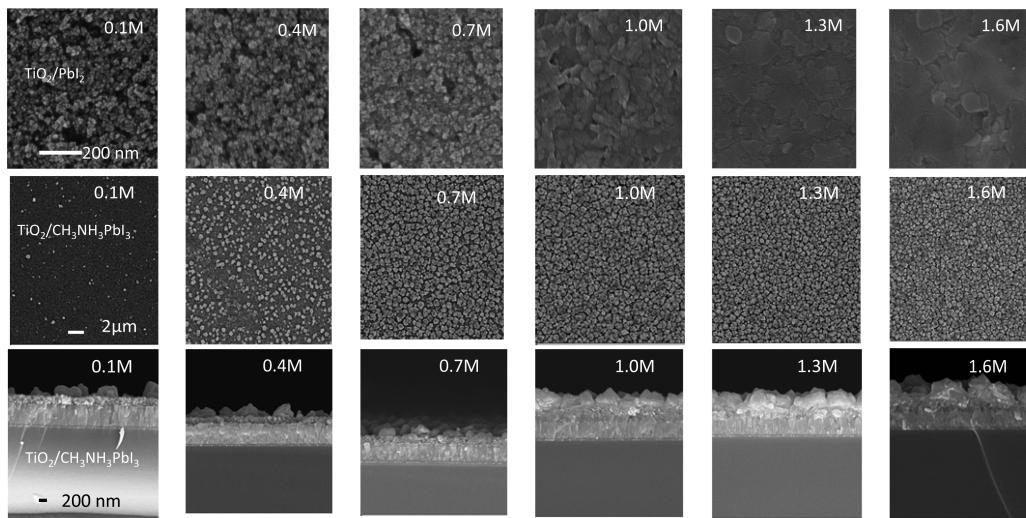


**Figure 1.** SEM top views of PbI<sub>2</sub>/m-TiO<sub>2</sub>/d-TiO<sub>2</sub>/FTO (the first row), CH<sub>3</sub>NH<sub>3</sub>PbI<sub>3</sub>/m-TiO<sub>2</sub>/d-TiO<sub>2</sub>/FTO (the second row), and cross sectional views of CH<sub>3</sub>NH<sub>3</sub>PbI<sub>3</sub>/m-TiO<sub>2</sub>/d-TiO<sub>2</sub>/FTO (the third row).

retard the charge recombination<sup>29</sup> and that the addition of DMSO into the PbI<sub>2</sub> solution can retard the PbI<sub>2</sub> crystallization.<sup>30</sup> The concentration of PbI<sub>2</sub> ( $C_{\text{PbI}_2}$ ) in the spin-coating solution is an important factor that affects the infiltration of the perovskite into the mesoporous layer and the amount of perovskite that is deposited. Here, we have investigated the effect of PbI<sub>2</sub> concentration on the solar cell performance, and use transient photovoltaic, photocurrent decay and time correlated single photon counting (TCSPC) to unravel the charge recombination mechanism and charge carriers kinetics in these systems.

## RESULTS AND DISCUSSION

To investigate the effect of  $C_{\text{PbI}_2}$  on CH<sub>3</sub>NH<sub>3</sub>PbI<sub>3</sub> film morphology, we first prepared CH<sub>3</sub>NH<sub>3</sub>PbI<sub>3</sub> films on mesoporous TiO<sub>2</sub> (m-TiO<sub>2</sub>) films by spin-coating PbI<sub>2</sub> solutions in DMF with concentrations of 0.1, 0.4, 0.7, 1.0, 1.3, and 1.6 M. Scanning electron microscopy was used for analysis of the samples. Top view of PbI<sub>2</sub>/m-TiO<sub>2</sub>/d-TiO<sub>2</sub>/FTO samples (Figure 1, first row) shows the gradual filling of pores in the TiO<sub>2</sub> film as the concentration is increased from 0.1 to 0.7 M. The 0.1 M sample looks similar to the unmodified mesoporous TiO<sub>2</sub> film, but clear evidence of filling is seen at 0.4 M. For 0.7 M, most pores appear to be filled, while for concentrations of 1.0 M and higher, an overstanding layer of PbI<sub>2</sub> on top of m-TiO<sub>2</sub> is apparent. Top and cross section views of the resulting CH<sub>3</sub>NH<sub>3</sub>PbI<sub>3</sub>/m-TiO<sub>2</sub>/d-TiO<sub>2</sub>/FTO samples (Figure 1, second and third row) demonstrate that the surface coverage of perovskite on m-TiO<sub>2</sub> increases with  $C_{\text{PbI}_2}$ , that is, it changes from sparse particles on top of the mesoporous TiO<sub>2</sub> film to a complete densely packed layer of crystalline perovskite particles, with a size of about 500 nm as  $C_{\text{PbI}_2}$  increases from 0.1 to 1.6 M. The thickness of the mesoporous TiO<sub>2</sub> layer (250–300 nm) was kept constant in this study.

Figure 2a shows diffuse reflectance spectra of CH<sub>3</sub>NH<sub>3</sub>PbI<sub>3</sub>/m-TiO<sub>2</sub>/d-TiO<sub>2</sub>/FTO samples. The reflectance decreases significantly from sample 0.1 to 0.7 M, while there is no big difference for sample 1.0, 1.3, and 1.6 M. This shows that the fraction of absorbed light reaches a plateau when  $C_{\text{PbI}_2}$  is 0.7 M. Higher concentration will lead to more deposition of

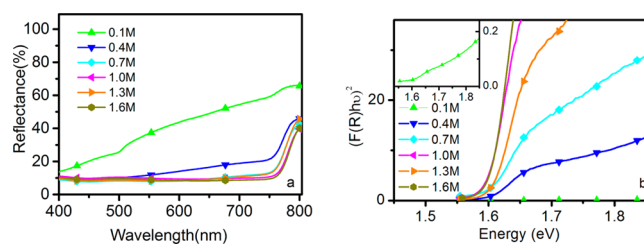


**Figure 2.** Diffuse reflectance spectra (a) and transformed Kubelka–Munk spectra (b) of CH<sub>3</sub>NH<sub>3</sub>PbI<sub>3</sub>/m-TiO<sub>2</sub>/d-TiO<sub>2</sub>/FTO samples using different  $C_{\text{PbI}_2}$ .

perovskite, but not to much more light absorption, but may affect the morphology of the resulting film. The transformed Kubelka–Munk spectrum is shown in Figure 2b, and the optical absorption coefficient ( $\alpha$ ) is calculated using reflectance data according to Kubelka–Munk equation,<sup>31</sup>  $F(R) = (\alpha) = (1 - R)^2/2R$ , where  $R$  is the fraction of reflected light. The incident photon energy ( $h\nu$ ) and the optical band gap energy ( $E_g$ ) are related to the transformed Kubelka–Munk function,  $[F(R)h\nu]^p = A(h\nu - E_g)$ , where  $E_g$  is the bandgap energy,  $A$  is the constant depending on transition probability, and  $p$  is the power index that is related to the optical absorption process, equal to 2 or 1/2 for direct or an indirect allowed transition, respectively. Herein, a direct transition is found and  $E_g$  of the perovskite samples are determined to be  $\sim 1.6$  eV for all, indicating a similar electronic structure of the perovskite samples prepared from different  $C_{\text{PbI}_2}$ .

Figure 3a shows photoluminescence spectra of the perovskite samples. A strong emission peak around 775 nm was observed for all the samples, except for the samples prepared from the lowest PbI<sub>2</sub> concentration that displayed only a weak and clearly blue-shifted emission. By increasing  $C_{\text{PbI}_2}$  from 0.1 to 1.0 M, the emission peak is shifted more to the near-infrared. At low  $C_{\text{PbI}_2}$  almost all of the perovskite is formed inside the mesoporous TiO<sub>2</sub> structure, where it has to form small crystals, which may show some quantum confinement effects. At higher  $C_{\text{PbI}_2}$ , the photoluminescence is likely to be dominated by the large perovskite crystals on top of the mesoporous structure that do not have quantum size effects. The 0.1 M sample shows

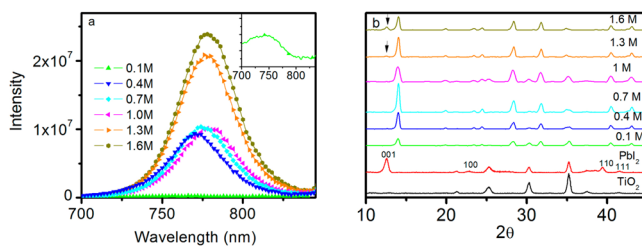


**Figure 3.** Photoluminescence spectra (a) of CH<sub>3</sub>NH<sub>3</sub>PbI<sub>3</sub>/m-TiO<sub>2</sub>/d-TiO<sub>2</sub>/FTO samples using different C<sub>PbI<sub>2</sub></sub>, and XRD (b) pattern of CH<sub>3</sub>NH<sub>3</sub>PbI<sub>3</sub>/m-TiO<sub>2</sub>/d-TiO<sub>2</sub>/ITO samples using different C<sub>PbI<sub>2</sub></sub>.

very weak emission, indicative of the lower amount of perovskite that is formed and the effective electron injection. The reflectance measurements (Figure 2a) show that the other samples except for 0.1 M show more or less the same diffuse reflectance; however, 1.3 and 1.6 M samples have a stronger photoluminescence, indicating a poorer electron injection, probably resulting from an impurity of PbI<sub>2</sub> in the perovskite or a perovskite layer that is thicker than the electron diffusion length, as will be discussed below.

Figure 3b shows the X-ray diffraction (XRD) pattern of the perovskite CH<sub>3</sub>NH<sub>3</sub>PbI<sub>3</sub> using different concentrations of PbI<sub>2</sub>. When PbI<sub>2</sub> is deposited on TiO<sub>2</sub>, it shows four peaks that are attributed to the (001), (100), (110), (111) lattice planes of a hexagonal (2H polytype; Inorganic Crystal Structure Database, collection code 68819). The predominant peak of (001) indicates that PbI<sub>2</sub> grows in a preferential orientation along the *c*-axis of the TiO<sub>2</sub> film. After dipping the PbI<sub>2</sub> into the CH<sub>3</sub>NH<sub>3</sub>I solution, we observe a series of new diffraction peaks that are in good agreement with literature data on the tetragonal phase of CH<sub>3</sub>NH<sub>3</sub>PbI<sub>3</sub> perovskite.<sup>32</sup> Comparing the perovskite samples, we can see that the 1.3 and 1.6 M samples have a small peak (indicated by an arrow in Figure 2) attributed to the (001) lattice plane of (2H) PbI<sub>2</sub>, indicating the existence of PbI<sub>2</sub> in this perovskite. The existence of PbI<sub>2</sub> may be caused by incomplete reaction of PbI<sub>2</sub> with CH<sub>3</sub>NH<sub>3</sub>I, as the PbI<sub>2</sub> layer becomes more compact when the PbI<sub>2</sub> concentration is higher than 1.0 M. We were not able to analyze the exact location of the residual PbI<sub>2</sub> in the film. Considering the two-step conversion process from PbI<sub>2</sub> to MAPbI<sub>3</sub>, it is most probable that residual PbI<sub>2</sub> appears on positions where access to MAI is most limited in the second step, that is, at the center of large crystals, or near the TiO<sub>2</sub> surface. This is in stark contrast to the work by Chen et al.,<sup>29</sup> where PbI<sub>2</sub> was formed upon annealing of fully converted MAPbI<sub>3</sub>, which was found to have a positive effect on photovoltaic performance. As PbI<sub>2</sub> has a higher conduction band than that of perovskite, the unreacted PbI<sub>2</sub> may in our case prevent electron injection from the perovskite into TiO<sub>2</sub>. This is consistent with the stronger emission found for these samples, as shown in Figure 3a.

In the *J*–*V* measurement of perovskite solar cells, an anomalous hysteresis has been reported by Snaith<sup>33</sup> and Grätzel.<sup>34</sup> It is reported that the anomalous hysteresis is affected by many factors, including solar cell structure, preparation condition, film thickness, and so on. The scanning speed and direction and light soaking can affect the resulting *J*–*V* measurement of perovskite solar cells significantly. In this work we investigated the effect of scan direction in the most efficient solar cell, prepared using 1 M PbI<sub>2</sub>. We do not see any large hysteresis effect, see Figure 4a. The *J*–*V* curves and IPCE spectra of Au/spiro-OMeTAD/CH<sub>3</sub>NH<sub>3</sub>PbI<sub>3</sub>/m-TiO<sub>2</sub>/d-

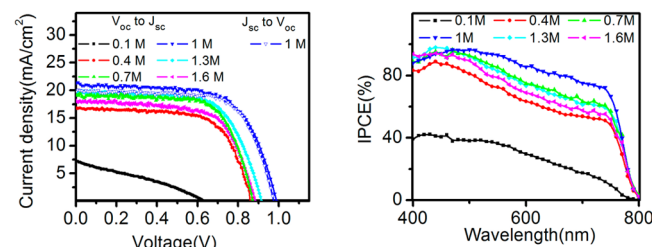


**Figure 4.** *J*–*V* curves under AM 1.5 illumination of 100 mW/cm<sup>2</sup> (using 50 mV/s to scan from V<sub>oc</sub> to J<sub>sc</sub> or J<sub>sc</sub> to V<sub>oc</sub> after a waiting time of 20 s at V<sub>oc</sub> or J<sub>sc</sub>) and IPCE spectra of Au/spiro-OMeTAD/CH<sub>3</sub>NH<sub>3</sub>PbI<sub>3</sub>/m-TiO<sub>2</sub>/d-TiO<sub>2</sub>/FTO solar cells using different C<sub>PbI<sub>2</sub></sub>.

TiO<sub>2</sub>/FTO using different concentrations of PbI<sub>2</sub> are shown in Figure 4. By using 0.1 M PbI<sub>2</sub>, the solar cell performance is extremely poor (1.4%), but by increasing the concentration to 0.4 M, the solar cell efficiency increases to 9.6%. A further increase of the PbI<sub>2</sub> concentration results first in an increase of the solar cell performance, followed by a decrease. The best performance of 13.9% was obtained using a PbI<sub>2</sub> concentration of 1.0 M. The IPCE shows a broader absorption when the PbI<sub>2</sub> concentration is increased from 0.1 to 0.4 M. The IPCE increase from 0.1 to 1.0 M is partially due to enhanced light harvesting, but is also affected by slower recombination, as will be discussed later. The decrease in IPCE from 1.0 to 1.6 M can be attributed to a decrease in charge injection efficiency due to residual PbI<sub>2</sub>, which may act as a barrier for electron injection at the TiO<sub>2</sub>/perovskite interface. From a whole view of the UV-vis, SEM, XRD, *J*–*V*, and IPCE, we can see that a concentration of 0.1 M PbI<sub>2</sub> is not enough to obtain sufficient pore filling in the TiO<sub>2</sub> by the perovskite and insufficient light is harvested in this system. A 0.4 M PbI<sub>2</sub> concentration increases the light harvesting in this system, while an increase of PbI<sub>2</sub> to 1.0 M enhanced light absorption further by the overstanding layer of perovskite crystals.

Small-modulation transient V<sub>oc</sub> decay experiments were used to measure the carrier lifetime. (Figure 5 a) In the device

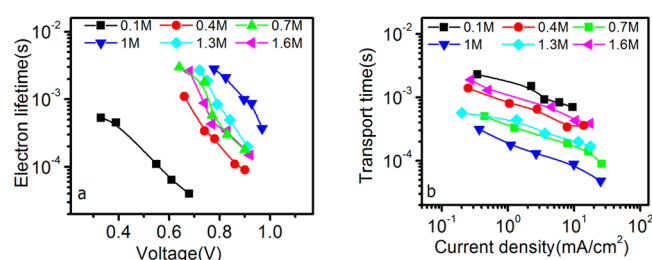


**Figure 5.** Electron lifetime and charge transport time of Au/spiro-OMeTAD/CH<sub>3</sub>NH<sub>3</sub>PbI<sub>3</sub>/m-TiO<sub>2</sub>/d-TiO<sub>2</sub>/FTO solar cells.

configuration used, we may assume that the measured lifetime is the electron lifetime ( $\tau_e$ ) in the mesoporous TiO<sub>2</sub>. This lifetime depends on the concentration of electrons and holes in the solar cell. Therefore, the electron lifetime is strongly influenced by the applied voltage or the light intensity. The measured  $\tau_e$  is shown as a function of open-circuit potential of the cells, obtained by varying the light intensity. The results shown are representative for typical devices for each condition. A decrease in  $\tau_e$  at higher light intensity (higher V<sub>oc</sub>) is attributed to faster recombination due to the increase in carrier concentration. Shortest lifetimes are found for the solar cells with the lowest perovskite coverage. In these cells, there will be

insufficient perovskite form complete coverage of the m-TiO<sub>2</sub> film, resulting in direct contact between TiO<sub>2</sub> and the HTM, which will lead to increased carrier recombination. The results suggest that coverage is already nearly complete for the 0.7 M device. Further increasing the PbI<sub>2</sub> concentration from 1.0 to 1.6 M leads to faster recombination. This confirms that the residual PbI<sub>2</sub> in the devices does not lead to a passivation effect, as contrast to findings by Chen et al.<sup>29</sup>

In Figure 5b, the small-modulation transient photocurrent decay is monitored under short-circuit conditions. The time constant is observed to decrease with increasing light intensity. Such dependence is normally observed in mesoporous TiO<sub>2</sub>-based DSSCs, as is explained by a multiple trapping/detrapping process. Interestingly, the transport time is longest for the 0.1 M devices, while the best performing solar cell (1.0 M) had the shortest transport time. As the mesoporous TiO<sub>2</sub> layer thickness is identical in all devices, it can be concluded that additional perovskite material can speed up the carrier transport. This can be attributed to the higher mobility in the perovskite compared to m-TiO<sub>2</sub>. Probably, electrons can hop back and forth between TiO<sub>2</sub> and perovskite. Further increasing the PbI<sub>2</sub> concentration from 1.0 to 1.6 M leads to longer electron transport times. This may be explained by a barrier of PbI<sub>2</sub> between the perovskite and the TiO<sub>2</sub>. This blocking layer may confine electron transport more to m-TiO<sub>2</sub> only, yielding slower transport. Such a barrier is, however, not consistent with the smaller electron lifetimes found for these devices. The lifetime and transport time measurement show that when a higher or lower concentration than 1.0 M PbI<sub>2</sub> is used more serious carrier recombination and slower charge transport occurs, resulting to a lower values of  $V_{oc}$  and  $J_{sc}$ , as was found shown in the analysis of the  $J-V$  curves.

Time correlated single photon counting (TCSPC) measurements were used to study the emission lifetime of perovskite on mesoporous TiO<sub>2</sub> and ZrO<sub>2</sub> using different  $C_{PbI_2}$  before (Figures 6 and 7a) and after (Figures 6 and 7b) coating with

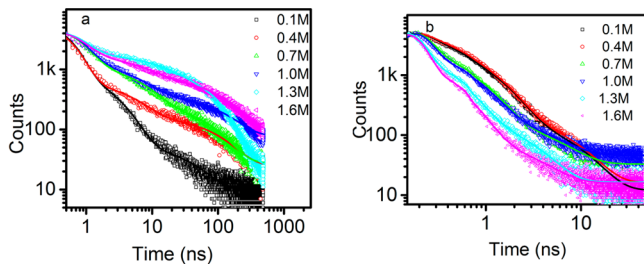


**Figure 6.** Normalized TCSPC measurements for CH<sub>3</sub>NH<sub>3</sub>PbI<sub>3</sub>/m-TiO<sub>2</sub>/d-TiO<sub>2</sub>/FTO samples before (a) and after coating spiro-OMeTAD (b). Excitation was 404 nm. Data are in symbols and fitting are in solid lines.

the HTM spiro-OMeTAD. In all cases, there was a dense TiO<sub>2</sub> underlayer. The emission decays were fitted using a multi-exponential function. About 90% of the total amplitudes of the lifetimes for the samples are mainly associated with the first two lifetimes. For the sake of clarity and simplicity, we will use an amplitude-weighted lifetime ( $\tau$ ) as shown in Table 1 and refer to this as the emission lifetime.<sup>35</sup> A marked increase of the emission lifetime of perovskite on mesoporous TiO<sub>2</sub> is found for the 1.3 and 1.6 M PbI<sub>2</sub> samples, in accordance with a decrease in electron injection due to a PbI<sub>2</sub> barrier at the perovskite/TiO<sub>2</sub> interface or to the increased thickness, larger

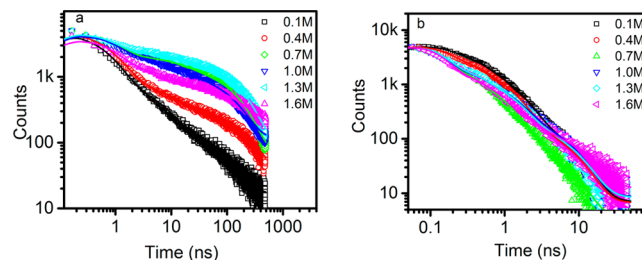


**Figure 7.** Normalized TCSPC measurements for CH<sub>3</sub>NH<sub>3</sub>PbI<sub>3</sub>/m-ZrO<sub>2</sub>/d-TiO<sub>2</sub>/FTO samples before (a) and after coating spiro-OMeTAD (b). Excitation was 404 nm. Data are in symbols and fitting are in solid lines.

**Table 1. Measured Lifetimes for the Emission Decays of Perovskite Samples on Mesoporous TiO<sub>2</sub> and ZrO<sub>2</sub> with and without Spiro-OMeTAD<sup>a</sup>**

	0.1 M	0.4 M	0.7 M	1.0 M	1.3 M	1.6 M
TiO <sub>2</sub> /CH <sub>3</sub> NH <sub>3</sub> PbI <sub>3</sub>	0.89	3.2	5.0	7.9	17.0	17.3
ZrO <sub>2</sub> /CH <sub>3</sub> NH <sub>3</sub> PbI <sub>3</sub>	3.4	10.2	38.9	27.4	54.3	26.4
$\tau_{inj,TiO_2/CH_3NH_3PbI_3}$	1.2	4.7	5.7	11.1	24.7	50.2
$\phi_{inj,TiO_2/CH_3NH_3PbI_3}$	74%	69%	87%	71%	69%	34%
TiO <sub>2</sub> /CH <sub>3</sub> NH <sub>3</sub> PbI <sub>3</sub> /spiro	0.56	0.61	0.23	0.19	0.10	0.085
ZrO <sub>2</sub> /CH <sub>3</sub> NH <sub>3</sub> PbI <sub>3</sub> /spiro	0.60	0.45	0.22	0.32	0.31	0.28
$\phi_{inj,ZrO_2/CH_3NH_3PbI_3/spiro}$	82%	96%	99%	99%	99%	99%

<sup>a</sup>Emission lifetimes are in ns. Also shown is the calculation electron injection time into TiO<sub>2</sub> (ns) and the injection efficiency.

than the electron diffusion length. Mesoporous ZrO<sub>2</sub> was used as a reference “inert” substrate for the perovskite samples. No electron injection from the perovskite into the conduction band of ZrO<sub>2</sub> can take place, because it is located at a much higher energy than the conduction band of perovskite. The emission lifetime of the perovskite on ZrO<sub>2</sub> was found to increase with PbI<sub>2</sub> concentration up to about 40 ns at 0.7 M. The shorter emission lifetimes found on the mesoporous TiO<sub>2</sub> substrates demonstrate electron injection from the perovskite to the TiO<sub>2</sub><sup>36</sup> competing with radiative recombination. TCSPC emission measurements of perovskite samples reported previously gave mono or biexponential decays with a time constants of 5.6 ns<sup>37</sup> and 9.6 ns<sup>36</sup> for CH<sub>3</sub>NH<sub>3</sub>PbI<sub>3</sub> and 283 ns for CH<sub>3</sub>NH<sub>3</sub>PbCl<sub>x</sub>I<sub>3-x</sub>.<sup>38</sup> The reason for different values found here can be attributed to different perovskite preparation procedures or measurement conditions (in vacuum or in air). As can be seen in Table 1, the electron injection time ( $\tau = 1/k_{inj}$ ,  $k_{TiO_2/perovskite} = k_{inj} + k_{emission}$ ,  $k_{emission} = k_{ZrO_2/perovskite}$ ), calculated from the emission lifetimes of perovskite on TiO<sub>2</sub> and ZrO<sub>2</sub> increases with  $C_{PbI_2}$ , from about 1 ns for the 0.1 M sample to 50 ns for the 1.6 M sample. The slower injection may be attributed to the difference in the amount of perovskite that is deposited and, thus, the longer electron diffusion length in the perovskite for thicker samples. The presence of a PbI<sub>2</sub> barrier layer between TiO<sub>2</sub> and perovskite, which may be present in samples prepared from higher PbI<sub>2</sub> concentrations, will also slow down electron injection. The quenching efficiency of the emission by TiO<sub>2</sub>, presumably equal to the electron injection efficiency, is about 70% for all samples, except for the 1.6 M sample for which it is lower (34%).

Addition of the spiro-OMeTAD adds another quenching interface to the system, due to hole injection from the perovskite. From the data of samples with mesoporous  $ZrO_2$ , the quenching efficiency of spiro-OMeTAD is calculated to be close to 100%, but somewhat lower for the 0.1 M sample (82%). This suggests that hole injection from the perovskite into spiro-OMeTAD is very efficient. The lower value the 0.1 M sample can be ascribed to incomplete pore filling of spiro-OMeTAD inside the mesoporous structure. Overall, carrier extraction from the perovskites at the contacts is thus expected to be very efficient in solar cell devices. For the 1.6 M device the p-contact appears to be the dominant active interface, while for the other devices both contacts are probable equally active, considering that illumination takes place from the  $TiO_2$  side. That said, emission quenching does not give direct information on charge separation and should be treated with care.

## CONCLUSION

By using different concentrations of  $PbI_2$  in the spin-coating step for a two-step method to fabricate  $CH_3NH_3PbI_3$  perovskite solar cell, a best solar cell performance of 13.9% was obtained using 1.0 M of  $PbI_2$ . Electron lifetime and transport time studies show slowest recombination and best carrier transport in these devices. Rapid quenching of the perovskite emission is found in device-like structures, suggesting reasonably good efficient carrier extraction at the  $TiO_2$  interface and quantitative extraction at the spiro-OMeTAD interface.

## ASSOCIATED CONTENT

### Supporting Information

Detailed description of preparation methods and characterization. Optical photographs of a spin-coated  $PbI_2$  layer and resulting perovskite layer. SEM cross sections of  $PbI_2$  films. This material is available free of charge via the Internet at <http://pubs.acs.org>.

## AUTHOR INFORMATION

### Corresponding Author

\*E-mail: gerrit.boschloo@kemi.uu.se.

### Notes

The authors declare no competing financial interest.

## ACKNOWLEDGMENTS

We thank the Swedish Energy Agency, the Swedish Research Council (VR), the Göran Gustafsson Foundation, the STandUP for Energy program, and the Knut and Alice Wallenberg Foundation for financial support.

## REFERENCES

- (1) Hagfeldt, A.; Grätzel, M. Light-Induced Redox Reactions in Nanocrystalline Systems. *Chem. Rev.* **1995**, *95*, 49–68.
- (2) Hodes, G. Perovskite-Based Solar Cells. *Science* **2013**, *342*, 317–318.
- (3) Papavassiliou, G. C. Three-and Low-Dimensional Inorganic Semiconductors. *Prog. Solid State Chem.* **1997**, *25*, 125–270.
- (4) Umebayashi, T.; Asai, K.; Kondo, T.; Nakao, A. Electronic Structures of Lead Iodide Based Low-Dimensional Crystals. *Phys. Rev. B* **2003**, *67*, 155405.
- (5) Eperon, G. E.; Stranks, S. D.; Menelaou, C.; Johnston, M. B.; Herz, L. M.; Snaith, H. J. Formamidinium Lead Trihalide: A Broadly Tunable Perovskite for Efficient Planar Heterojunction Solar Cells. *Energy Environ. Sci.* **2014**, *7*, 982–988.
- (6) Koh, T. M.; Fu, K.; Fang, Y.; Chen, S.; Sum, T. C.; Mathews, N.; Mhaisalkar, S. G.; Boix, P. P.; Baikie, T. Formamidinium-Containing Metal-Halide: An Alternative Material for Near-IR Absorption Perovskite Solar Cells. *J. Phys. Chem. C* **2013**, *118*, 16458–16462.
- (7) Pang, S.; Hu, H.; Zhang, J.; Lv, S.; Yu, Y.; Wei, F.; Qin, T.; Xu, H.; Liu, Z.; Cui, G.  $NH_2CH=NH_2PbI_3$ : An Alternative Organolead Iodide Perovskite Sensitizer for Mesoscopic Solar Cells. *Chem. Mater.* **2014**, *26*, 1485–1491.
- (8) Im, J. H.; Chung, J.; Kim, S. J.; Park, N. G. Synthesis, Structure, and Photovoltaic Property of A Nanocrystalline 2H Perovskite-type Novel Sensitizer ( $CH_3CH_2NH_3PbI_3$ ). *Nanoscale* **2012**, *7*, 353.
- (9) Pellet, N.; Gao, P.; Gregori, G.; Yang, T.-Y.; Nazeeruddin, M. K.; Maier, J.; Grätzel, M. Mixed-Organic-Cation Perovskite Photovoltaics for Enhanced Solar-Light Harvesting. *Angew. Chem., Int. Ed.* **2014**, *53*, 3151–3157.
- (10) Ogomi, Y.; Morita, A.; Tsukamoto, S.; Saitho, T.; Fujikawa, N.; Shen, Q.; Toyoda, T.; Yoshino, K.; Pandey, S. S.; Ma, T.; Hayase, S.  $CH_3NH_3Sn_xPb_{(1-x)}I_3$  Perovskite Solar Cells Covering up to 1060 nm. *J. Phys. Chem. Lett.* **2014**, *5*, 1004–1011.
- (11) Edri, E.; Kirmayer, S.; Cahen, D.; Hodes, G. High Open-Circuit Voltage Solar Cells Based on Organic–Inorganic Lead Bromide Perovskite. *J. Phys. Chem. Lett.* **2013**, *4*, 897–902.
- (12) Cai, B.; Xing, Y. D.; Yang, Z.; Zhang, W. H.; Qiu, J. S. High Performance Hybrid Solar Cells Sensitized by Organolead Halide Perovskites. *Energy Environ. Sci.* **2013**, *6*, 1480–1485.
- (13) Suarez, B.; Gonzalez-Pedro, V.; Ripolles, T. S.; Sanchez, R. S.; Otero, L.; Mora-Sero, I. Recombination Study of Combined Halides (Cl, Br, I) Perovskite Solar Cells. *J. Phys. Chem. Lett.* **2014**, *5*, 1628–1635.
- (14) Aharon, S.; Cohen, B. E.; Etgar, L. Hybrid Lead Halide Iodide and Lead Halide Bromide in Efficient Hole Conductor Free Perovskite Solar Cell. *J. Phys. Chem. C* **2014**, *118*, 17160–17165.
- (15) Conings, B.; Baeten, L.; De Dobbelaere, C.; D’Haen, J.; Manca, J.; Boyen, H. G. Perovskite-Based Hybrid Solar Cells Exceeding 10% Efficiency with High Reproducibility Using a Thin Film Sandwich Approach. *Adv. Mater.* **2014**, *26*, 2041–2046.
- (16) Research Cell Efficiency Records. NREL (<http://www.nrel.gov/ncpv/>), 2014.
- (17) Kim, H. S.; Lee, C. R.; Im, J. H.; Lee, K. B.; Moehl, T.; Marchioro, A.; Moon, S. J.; Humphry-Baker, R.; Yum, J. H.; Moser, J. E.; Grätzel, M.; Park, N. G. Lead Iodide Perovskite Sensitized All-Solid-State Submicron Thin Film Mesoscopic Solar Cell with Efficiency Exceeding 9%. *Sci. Rep.* **2012**, *2*, 591.
- (18) Lee, M. M.; Teuscher, J.; Miyasaka, T.; Murakami, T. N.; Snaith, H. J. Efficient Hybrid Solar Cells Based on Meso-Superstructured Organometal Halide Perovskites. *Science* **2012**, *338*, 643–647.
- (19) Bi, D.; Yang, L.; Boschloo, G.; Hagfeldt, A.; Johansson, E. M. J. Effect of Different Hole Transport Materials on Recombination in  $CH_3NH_3PbI_3$  Perovskite-Sensitized Mesoscopic Solar Cells. *J. Phys. Chem. Lett.* **2013**, *4*, 1532–1536.
- (20) Bi, D.; Boschloo, G.; Schwarzmüller, S.; Yang, L.; Johansson, E. M. J.; Hagfeldt, A. Efficient and Stable  $CH_3NH_3PbI_3$ -Sensitized ZnO Nanorod Array Solid-State Solar Cells. *Nanoscale* **2013**, *5*, 11686–11691.
- (21) Leijtens, T.; Lauber, B.; Eperon, G. E.; Stranks, S. D.; Snaith, H. J. The Importance of Perovskite Pore Filling in Organometal Mixed Halide Sensitized  $TiO_2$ -Based Solar Cells. *J. Phys. Chem. Lett.* **2014**, *5*, 1096–1102.
- (22) Eperon, G. E.; Burlakov, V. M.; Docampo, P.; Goriely, A.; Snaith, H. J. Morphological Control for High Performance, Solution-Processed Planar Heterojunction Perovskite Solar Cells. *Adv. Funct. Mater.* **2014**, *24*, 151–157.
- (23) Liu, M. Z.; Johnston, M. B.; Snaith, H. J. Efficient Planar Heterojunction Perovskite Solar Cells by Vapour Deposition. *Nature* **2013**, *501*, 395.
- (24) Malinkiewicz, O.; Yella, A.; Lee, Y. H.; Espallargas, G. M.; Grätzel, M.; Nazeeruddin, M. K.; Bolink, H. J. Perovskite Solar Cells Employing Organic Charge-Transport Layers. *Nat. Photonics* **2014**, *8*, 128–132.

- (25) Chen, Q.; Zhou, H.; Hong, Z.; Luo, S.; Duan, H.-S.; Wang, H.-H.; Liu, Y.; Li, G.; Yang, Y. Planar Heterojunction Perovskite Solar Cells via Vapor-Assisted Solution Process. *J. Am. Chem. Soc.* **2013**, *136*, 622–625.
- (26) Liang, K. N.; Mitzi, D. B.; Prikas, M. T. Synthesis and Characterization of Organic–Inorganic Perovskite Thin Films Prepared Using a Versatile Two-Step Dipping Technique. *Chem. Mater.* **1998**, *10*, 403–411.
- (27) Burschka, J.; Pellet, N.; Moon, S. J.; Humphry-Baker, R.; Gao, P.; Nazeeruddin, M. K.; Gratzel, M. Sequential Deposition as a Route to High-Performance Perovskite-Sensitized Solar Cells. *Nature* **2013**, *499*, 316.
- (28) Bi, D. Q.; Moon, S. J.; Haggman, L.; Boschloo, G.; Yang, L.; Johansson, E. M. J.; Nazeeruddin, M. K.; Gratzel, M.; Hagfeldt, A. Using A Two-Step Deposition Technique to Prepare Perovskite ( $\text{CH}_3\text{NH}_3\text{PbI}_3$ ) for Thin Film Solar Cells Based on  $\text{ZrO}_2$  and  $\text{TiO}_2$  Mesostuctures. *RSC Adv.* **2013**, *3*, 18762–18766.
- (29) Chen, Q.; Zhou, H.; Song, T.-B.; Luo, S.; Hong, Z.; Duan, H.-S.; Dou, L.; Liu, Y.; Yang, Y. Controllable Self-Induced Passivation of Hybrid Lead Iodide Perovskites toward High Performance Solar Cells. *Nano Lett.* **2014**, *14*, 4158–4163.
- (30) Wu, Y.; Islam, A.; Yang, X.; Qin, C.; Liu, J.; Zhang, K.; Peng, W.; Han, L. Retarding the Crystallization of  $\text{PbI}_2$  for Highly Reproducible Planar-Structured Perovskite Solar Cells via Sequential Deposition. *Energy Environ. Sci.* **2014**, *7*, 2934–2938.
- (31) Lin, H.; Huang, C. P.; Li, W.; Ni, C.; Shah, S. I.; Tseng, Y.-H. Size Dependency of Nanocrystalline  $\text{TiO}_2$  on Its Optical Property and Photocatalytic Reactivity Exemplified by 2-Chlorophenol. *Appl. Catal. B: Environ.* **2006**, *68*, 1–11.
- (32) Baikie, T.; Fang, Y. N.; Kadro, J. M.; Schreyer, M.; Wei, F. X.; Mhaisalkar, S. G.; Graetzel, M.; White, T. J. Synthesis and Crystal Chemistry of The Hybrid Perovskite ( $\text{CH}_3\text{NH}_3$ )  $\text{PbI}_3$  for Solid-State Sensitised Solar Cell Applications. *J. Mater. Chem. A* **2013**, *1*, 5628–5641.
- (33) Snaith, H. J.; Abate, A.; Ball, J. M.; Eperon, G. E.; Leijtens, T.; Noel, N. K.; Stranks, S. D.; Wang, J. T.-W.; Wojciechowski, K.; Zhang, W. Anomalous Hysteresis in Perovskite Solar Cells. *J. Phys. Chem. Lett.* **2014**, *5*, 1511–1515.
- (34) Dualeh, A.; Moehl, T.; Tétreault, N.; Teuscher, J.; Gao, P.; Nazeeruddin, M. K.; Grätzel, M. Impedance Spectroscopic Analysis of Lead Iodide Perovskite-Sensitized Solid-State Solar Cells. *ACS Nano* **2013**, *8*, 362–373.
- (35) Lakowicz, J. R. *Principles of Fluorescence Spectroscopy*; Springer: New York, 2006.
- (36) Marchioro, A.; Teuscher, J.; Friedrich, D.; Kunst, M.; van de Krol, R.; Moehl, T.; Grätzel, M.; Moser, J.-E. Unravelling the Mechanism of Photoinduced Charge Transfer Processes in Lead Iodide Perovskite Solar Cells. *Nat. Photonics* **2014**, *8*, 250–255.
- (37) Xing, G.; Mathews, N.; Sun, S.; Lim, S. S.; Lam, Y. M.; Grätzel, M.; Mhaisalkar, S.; Sum, T. C. Long-Range Balanced Electron-and Hole-Transport Lengths in Organic-Inorganic  $\text{CH}_3\text{NH}_3\text{PbI}_3$ . *Science* **2013**, *342*, 344–347.
- (38) Stranks, S. D.; Eperon, G. E.; Grancini, G.; Menelaou, C.; Alcocer, M. J. P.; Leijtens, T.; Herz, L. M.; Petrozza, A.; Snaith, H. J. Electron-Hole Diffusion Lengths Exceeding 1 Micrometer in an Organometal Trihalide Perovskite Absorber. *Science* **2013**, *342*, 341–344.